International Journal of Pharmaceutics 644 (2023) 123319

Contents lists available at ScienceDirect

International Journal of Pharmaceutics

journal homepage: www.elsevier.com/locate/ijpharm

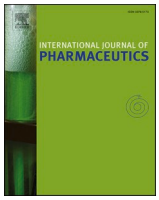

Assessing the physicochemical stability and intracellular trafficking of mRNA-based COVID-19 vaccines

Benedetta Fongaro [a], Benedetta Campara [a], Giulia Yuri Moscatiello [b], Ada De Luigi [b], Davide Panzeri [d], Laura Sironi [d], Paolo Bigini [b], Giovanni Carretta [c], Giorgia Miolo [a], Gianfranco Pasut [a,*], Patrizia Polverino De Laureto [a,*]

[a] Department of Pharmaceutical and Pharmacological Sciences, University of Padova, via F. Marzolo, 5, Padova, Italy
[b] Department of Biochemistry and Molecular Biology, Mario Negri Institute for Pharmacological Research IRCCS, Via Mario Negri 2, Milano, Italy
[c] Azienda ULSS 3 Serenissima, Via Don Federico Tosatto, 147, Venezia, Italy
[d] Department of Physics, University of Milano Bicocca, Piazza dell'Ateneo Nuovo, 1, Milano, Italy

ARTICLE INFO

Keywords:
mRNA-based COVID-19 Vaccines
Solid lipid nanoparticles
Light stress
Thermal stress
Physicochemical stability

ABSTRACT

The emergence of SARS-CoV-2 in Wuhan, China in 2019 has had a profound impact on humanity in every facet. While vaccines against this viral pathogen have been approved a year later, limitations to this therapeutic intervention persist, such as drug sensitivity to transportation and storage conditions, as well as significant financial losses from non-injected resuspended vials.

Our research delves into the effects of thermal denaturation (4 – 40 °C) and light irradiation (720 and 10460 kJ/m^2) on the mRNA-based vaccines BNT162b2 from BioNTech/Pfizer and mRNA-1273 from Moderna. We also investigated vaccine stability following incubation in syringes to simulate potential interactions with silicon oil. By assaying the effects of these stressors via biochemical and biophysical methods, we aim to elucidate the physicochemical properties, integrity, and stability of these mRNA-based vaccines.

Furthermore, the incorporation of a fluorophore into both vaccines allowed us to monitor their localization within cells and assess their capacity to evade vesicular transport mechanisms, thus evaluating the differences between the two formulations.

A comprehensive understanding of the aforementioned attributes can enable the establishment of optimal storage and manipulation conditions for these vaccines, thereby ensuring their safe and efficacious application while minimizing the waste of functional and safe therapeutic agents.

1. Introduction

At the end of 2019, humanity has started to face a new coronavirus, named SARS-CoV-2 (Zhu et al., 2020). This virus, never previously identified in humans was isolated in Wuhan, China, and has been responsible for the COVID-19 pandemic. Beside several strategies to prevent the spread of the virus, vaccination represented the most promising intervention that at the same time allowed combating this pandemic.

The European Medicines Agency (EMA) approved five vaccinations for the treatment of SARS-CoV-2: BNT162b2 from BioNTech/Pfizer, mRNA-1273 from Moderna, AZD1222 from AstraZeneca/Oxford University, Ad26.COV2.S from Janssen/Johnson & Johnson and NVX-CoV2373 from Novavax. Among these two vaccines were based on mRNA technology, the Pfizer mRNABNT162b2 (Comirnaty) and COVID-19 Vaccine Moderna mRNA-1273 vaccines (Spikevax) (Polack et al., 2020).

These vaccines showed about 95% efficacy for the prevention of a SARS-CoV-2-infection (Polack et al., 2020). They consist of single mRNA strand, encapsulated in solid lipid nanoparticles (SLNs), measure 60–100 nm and contain approximately 100 mRNA molecules per lipid nanoparticle (Arteta et al., 2018). They are administered by intramuscular injection into the deltoid muscle (Schoenmaker et al., 2021) (Fig. 1). Pfizer and Moderna vaccines specifically use nucleoside-modified mRNA, which reduces the inherent mRNA immunogenicity (Granados-Riveron and Aquino-Jarquin, 2021). They encode the mutated viral Spike (S) glycoprotein used by the coronavirus SARS-CoV-2 to enter cells (Duan et al., 2020). After the intramuscular injection, the

* Corresponding authors.
E-mail addresses: gianfranco.pasut@unipd.it (G. Pasut), patrizia.polverinodelaureto@unipd.it (P. Polverino De Laureto).

https://doi.org/10.1016/j.ijpharm.2023.123319
Received 27 June 2023; Received in revised form 1 August 2023; Accepted 14 August 2023
Available online 15 August 2023

mRNA can be transfected into the host cells and processed in the ribosomes. The mRNA is translated into the spike protein, which acts as an antigen and leads to development of an immune response to the virus.

Pfizer and Moderna vaccines have been similarly engineered with some differences in the composition of ionizable cation lipid and PEG-lipid. The ionizable lipid in Pfizer is [(4-hydroxybutyl)azanediyl]di (hexane-6,1-diyl) bis(2-hexyldecanoate) (ALC-0315), while that in Moderna is heptadecan-9-yl 8-{(2-hydroxyethyl)[6-oxo-6-(undecyloxy) hexyl]amino}octanoate (SM-102) (Fig. 1D). PEG-lipids affect many aspects of the SLN vaccines and have a role in RNA encapsulation efficiency and pharmacokinetics and pharmacodynamics parameters (circulation half-life, in vivo distribution, transfection efficiency, immune response) and formulation stability. The different properties strongly depend on the molecular structures of different PEG-lipids and on the ratio with other components in the final formulation (Hald Albertsen et al., 2022). The phospholipid distearoylphosphatidylcholine (DSPC) and cholesterol help to pack the cargo into the SLNs. The molar ratios of the cationic lipid:PEG-lipid: cholesterol: DSPC are (46.3:1.6:42.7:9.4) for the Pfizer and (50:1.5:38.5:10) for the Moderna vaccine (Schoenmaker et al., 2021). SLNs are considered pharmacologically inactive and minimally toxic since natural lipids are contained in these carriers (Alameh et al., 2022; Kulkarni et al., 2018).

SLNs, as an efficient delivery system, consist of some essential components, such as an ionizable cationic lipid, which promotes the formation of a complex with the negatively charged mRNA and allows the release of mRNA to the cytoplasm, and auxiliary lipids. These last species are lipid-linked polyethylene glycol (PEG)s, which increase the half-life of formulation and prevent aggregation during storage; cholesterol, a stabilizing agent; and naturally occurring phospholipids, which support lipid bilayer structure (Pardi et al., 2018; Ramachandran et al., 2022). The use of SLNs as mRNA deliver system to the cytosol has several advantages. SLNs protect the mRNA from the degradative action of ribonucleases (RNases) in vivo (Geall et al., 2012). They prolong the blood circulation time of the vaccine by reducing their clearance mediated by the kidneys and the mononuclear phagocyte system. Finally, an organ selectivity can be achieved adjusting the proportions of lipid components (Kowalski et al., 2019).

As in the case of biopharmaceuticals, vaccines are complex biological systems that require careful storage at very low temperature and handling precautions to ensure their stability and efficacy. They suffer of instability and can undergo chemical and physical degradation, concerning either the mRNA, the SLN carrier or both. One of the reasons for the instability is due to the peculiar structure of these SLNs consisting in a core composed by mRNA, cation lipid and water while the helper lipids are in the outer layer (Schoenmaker et al., 2021). Chemical instability derives from reactions of hydrolysis or oxidation. For example, at the level of SLN, the carboxyl-ester group of the phosphatidylcholine, as in DSPC and the ionizable cationic lipids, are susceptible to hydrolysis, which can be accelerated by eventual changes in pH and temperature. In the case of mRNA, hydrolysis can involve the phosphodiester bonds in its backbone. SLNs and mRNAs are then susceptible of oxidation, which could alter completely their structure determining an inefficacy of the

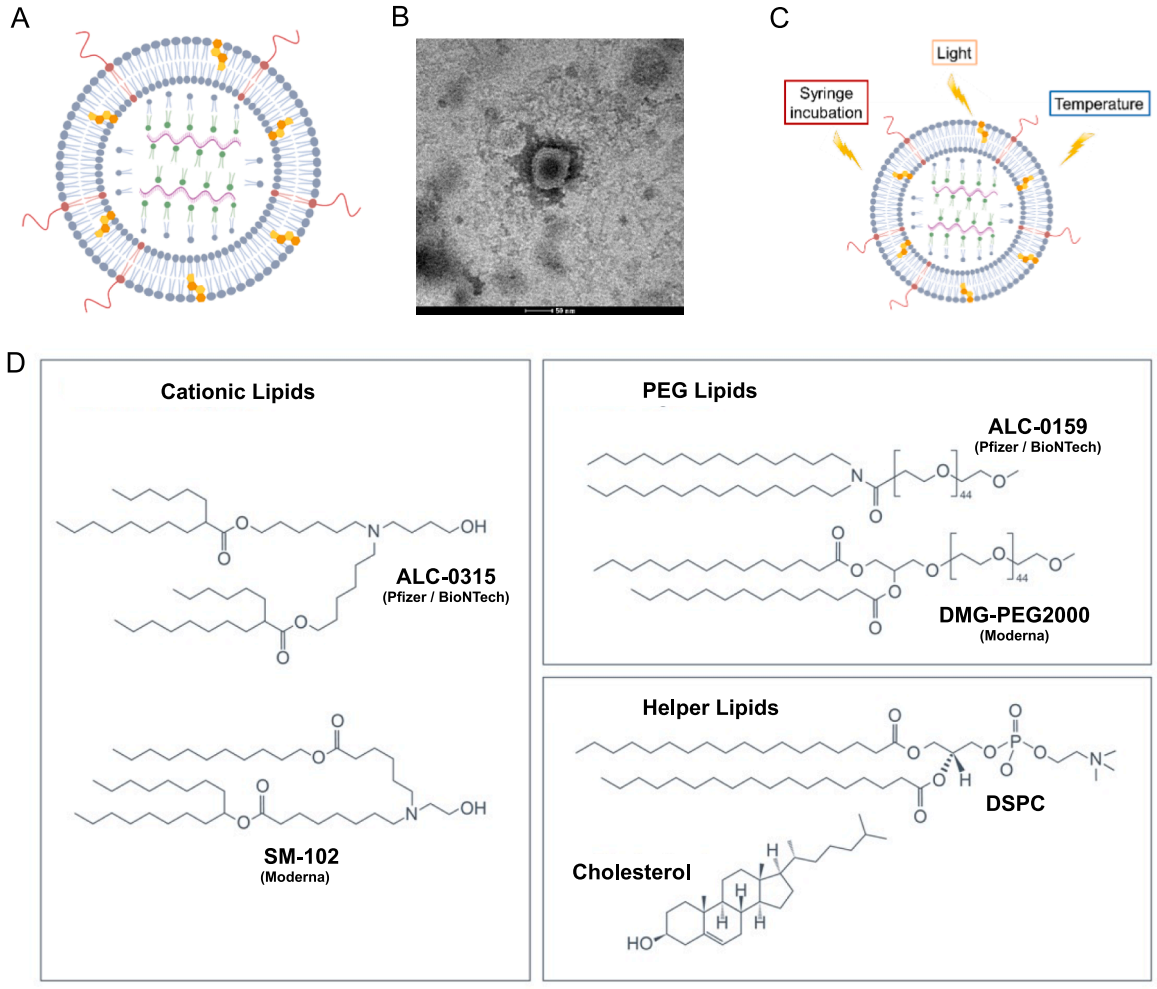

Fig. 1. Design of mRNA-SLN vaccine structure (A), TEM image of Pfizer vaccine (scale bar in TEM picture corresponds to 50 nm.) (B), stress factors used in this work (C), and chemical structure of lipids used in the mRNA vaccines (Tenchov et al., 2021).

vaccine.

The physical degradation phenomena are aggregation, precipitation, and adsorption. Aggregation can occur during all stages of the lifetime of the vaccine, including purification, sterilization, shipping, storage, and delivery processes. One of the main causes of possible instability of the mRNA SLN- SARS-CoV-2 vaccines is the storage at low temperatures. Possible stress factors, which could lead to a decreased stability of the vaccines are shown in Fig. 1.

Photostability is an important feature that is normally tested in the case of new biopharmaceuticals. Since these drugs are exposed to light at different stages of their development, from the manufacturing to the shipping and drug administration, photostability testing is an integral part of stress testing of new drugs. ICH Q1B guidelines recommend specific conditions for these studies by using $<1.2 \times 10^6$ lux-hour in the visible region and <200 W·h/m^2 for the UV light (https://database.ich.org/sites/default/files/Q1B Guideline.pdf). No information is available on the photosensitivity of mRNA-vaccines exposed directly to light.

Furthermore, the most widely used RNA vaccines, Pfizer and Moderna, were labelled with DiD fluorophore for investigating the cell internalization pattern and the endosomal escape process looking for potential differences in correlation to their physical–chemical properties.

2. Materials and methods

2.1. Materials

Vaccines BNT162b2 and mRNA-1273 are provided from ULSS 3, Venice Hospital. They are vaccine residues prepared in hospital for the application to the patient by dilution of the commercial ones in aseptic conditions as indicated in the instruction on the leaflet. The samples have been used within the 6–8 h after the preparation. Agarose powder, Tris, acetic acid solution, EDTA were purchased from Sigma Aldrich. Lambda DNA Hind III Digest for DNA electrophoresis loaded as standard, gel loading buffer (0.05% bromophenol blue, 40% sucrose, 0.1 M EDTA, pH 8.0 and 0.5% SDS) and GelRed Nucleic Acid Stain used as fluorescent intercalating agent were obtained from Merck. Vybrant™ DiD Cell-Labeling solution was acquired from ThermoFisher.

2.2. Dynamic light scattering (DLS)

DLS measurements were performed on a Zetasizer Ultra (ZSU5700, Malvern instruments, Worcestershire, UK). Sample aliquots were loaded without dilutions. Each measurement is the result of the media between three runs. Scattering data were analyzed with the ZS Xplorer software and expressed as volume, number, and intensity size distributions from which the values of hydrodynamic diameter were extracted. The appropriate attenuator position was automatically determined by the Zetasizer instrument during the measurement sequence. Particularly, the attenuator factor applied by the instrument was 4 and 3, for all Pfizer and Moderna's measurements, respectively.

2.3. Transmission electron microscopy (TEM)

All analyses were performed by negative staining method, in which aliquots of 5 μL of the leftover liquid from diluted vaccines within the original glass vials were absorbed on the plastic grid. After 2 min, the excess solution was removed with filter paper. Grids were air-dried, stained with 10 μL of 1.0% (w/v) uranyl acetate solution for 7 min, washed in MilliQ water, and allowed to dry. Grids were examined by a Tecnai G2 12 Twin TEM microscope (FEI Company, Hillsboro, OR, USA). Size distribution of samples was calculated on 100 particles manually extracted from the micrographs using ImageJ software. Only clearly defined spherical and isolated particles were selected.

2.4. Spectroscopic measurements

UV–Vis analyses were performed by a Lambda-25 spectrophotometer (Perkin Elmer, Shelton, CT, USA) in a 230–350 or 230–500 nm range, using a quartz cuvette with a 1 cm pathlength and a sample dilution of 1:20 (Moderna) or 1:4 (Pfizer) in water. Spectra were taken at scan speed of 200 nm/min, data pitch of 0.1 nm. Circular dichroism (CD) measurements were performed on the samples diluted 1:3 (Moderna) and 1:2 (Pfizer) in water in the same conditions used for the stress tests to monitor the mRNA secondary and tertiary structure, by acquiring spectra in the 210–350 nm range by a Jasco J-810 spectropolarimeter (Tokyo, Japan). CD spectra were obtained using quartz cells with a 1 mm pathlength. CD signal was expressed as the degree of ellipticity.

2.5. Quantification of RNA by fluorescence-Based assays

The AccuBlue® Broad Range RNA Quantitation Kit (Biotium, Fremont, California) was used to quantify purified RNA samples and prepared according to the manufactory. The RNA Broad Range Dye was diluted in RNA Broad Range Buffer at a 1:200 ratio (working solution). A set of RNA standards was prepared by diluting RNA Broad Range Standard (100 ng/μL) in RNA Dilution Buffer generating a standard curve, where the fluorescence values were plotted as a function of total ng RNA/well. 10 μL of RNA standard or vaccine samples were mixed with 200 μL of the working solution and then incubated for 5–10 min in the dark before measurements. Fluorescence was measured using a Perkin Elmer Victor Nivo Multimode Microplate Reader (Waltham, Massachusetts, United States) set to 570 nm excitation and 630 nm emission. Measurements were performed in triplicate.

2.6. Agarose gel electrophoresis

Agarose gel electrophoresis was performed to evaluate the physical stability of mRNA after exposure to stressors. An 1.0% (*w/v*) agarose solution in 40 mM Tris, 20 mM acetic acid and 1 mM EDTA(TAE) buffer at pH 8.0 was boiled and then poured within the gel cassette after the gel temperature of 65 °C was reached. The resulting gel was allowed to air dry. The samples were prepared by mixing an amount of vaccine LNP with the gel loading buffer (0.05% bromophenol blue, 40% sucrose, 0.1 M EDTA, pH 8.0 and 0.5% SDS), to favor the disassembling of LNP and releasing the mRNA and diluting this solution with TAE buffer to a final volume of 15 μL. Samples were loaded on the gel and the electrophoretic run was performed in TAE buffer. After the run, the gel was kept in a solution of GelRed Nucleic Acid Stain (Sigma Aldrich) for one hour and visualized with a UV-transilluminator.

2.7. RP-HPLC

Reverse Phase (RP)-HPLC analyses were carried out on a High-Performance Liquid Chromatography (HPLC) (Agilent 1290 system, Santa Clara, CA, USA) system, using a Jupiter C18 column (4.6 mm × 150 mm, 5.0 μm; Phenomenex, Torrence, CA, USA) at column temperature of 50 °C and sample temperature of 25 °C. Lipids were eluted using binary linear gradients starting from a mixture of 15% A and 85% B to 100% B in 18 min followed by a 2-min plateau at 100% B, where A is 0.1% (v/v) TFA in water and B is 0.1% (v/v) TFA in methanol. The chromatogram was monitored at 205 nm. The mobile phase composition was then changed back to initial solvent mixture and the column was equilibrated for 10 min before every subsequent run. The flow rate of the mobile phase was set to 1 mL/min. All chromatographic analyses were performed in triplicate.

2.8. Exposure to stressors

Thermal stress. Non diluted mRNA-SLN-vaccine residues from different original vials (same batch) were mixed, transferred into glass

vials, and placed in a Stability Test Chamber at 40 °C, 60% relative humidity (RH) for 8 days. On the 4th and 8th days, dynamic light scattering (DLS) measurements were performed to assess the potential degradation or aggregation phenomena occurring at the nanoparticles in comparison to the unstressed samples.

Incubation in syringe. Non diluted mRNA-SLN-vaccine residues from different original vials (same batch) were mixed and transferred into disposable sterile syringes for 90 min at room temperature. In order to evaluate if silicon oil present inside the syringes could trigger physical instability phenomena to nanoparticles, DLS measurements of the solutions were performed at different time points (10, 40 and 90 min) and compared to the untreated vaccines used as reference.

Exposure to artificial sunlight. The stability of vaccines was tested after artificial solar light irradiation using a SunTest CPS + instrument (Atlas Material Testing Technologies GmbH, Linsengericht, Germany). The analyses were performed in accordance with the ICH Q1B guidelines (https://database.ich.org/sites/default/files/Q1B Guideline.pdf). The vaccines were irradiated in non-diluted form. Non-irradiated (dark) samples were used as a control. Two different doses of artificial solar light were applied: 720 kJ/m^2 (200 W hours/m^2) in the UV region (320–400 nm) as indicated in ICH Q1B guidelines; 10460 kJ/m^2 that was applied to maximize the light stressor, following the exposure criteria for "stress test" photostability studies, namely until significant degradation has occurred. The temperature was controlled by using a SunCool® device and kept at 22 °C.

2.9. Cell culture

Cells used for this work are A549 cells, human lung adenocarcinoma epithelial cells. They were cultured in Medium Dulbecco's Modified Eagle (DMEM) and 10% Fetal Calf Serum (FCS), 1% L-glutamine and 1% penicillin/streptomycin maintained at 37 °C in a humified atmosphere in the presence of 5% CO_2.

2.10. Treatment with Pfizer and Moderna SLNs

Vaccine formulations were labelled by using DiD cell-labelling solution and the same procedure described in the manufacturer's instructions for cells labelling. The labelled SLNs solutions were diluted to 2.5 μg/ml with PBS 1 ×. A549 cells were seeded in a 12-well plate (Corning Costar) with a ø19 mm cover glass (VWR, Avantor) for each well and 24 h later they were treated with the solution of vaccines into the media. The incubation lasted 3, 24 and 96 h at 37 °C in a humified atmosphere in the presence of 5% CO_2.

2.11. WGA and Hoechst 33,258 staining and images acquisition

A549 cells were fixed with 4% PAF for 10 min at room temperature and membrane glycoproteins were stained with Wheat Agglutinin Germ (WGA) 488 (Invitrogen, Thermo Fisher Scientific W11261) diluted 1:200 for 10 min at room temperature. We then stained cell nuclei with Hoechst 33,258 (Sigma-Aldrich 23491–45-4) at 2 μg/ml concentration for 10 min at room temperature. Fluoromount Aqueous Mounting Medium (Merck, Sigma-Aldrich F4680) was used to mount glasses. Images were acquired at Virtual Slide Olympus VS120 microscope associated with a system of confocal microscopy to enable us to separate the wavelengths emission signals obtained by laser excitation at 488 nm (green signal related to the WGA) and 546 nm (red signal related to the DiD). Moreover, to furthermore verify if the fluorescence signal recovered in vitro was specific for both vesicles and fluorescent vaccines respectively, the signal associated with the vaccines was visualized before WGA incubation.

2.12. Image Processing and quantification

The so acquired images were analysed to quantify and measure the Pearson correlation coefficient "r" between the green signal of the intracellular vesicles and the red signal of the vaccines. The images acquired by the Olympus Virtual Slide Microscope VS120-S6-W were saved in the Olympus-CellSense proprietary file format (.vsi). Data was converted into OME-TIFF format by an automated Bash script which exploits command-line bindings to access the Bioformats framework (Linkert et al., 2010). From the converted images, five 3000 × 3000 pixels (~1000 μm^2) random regions of interest (ROIs) were selected for each time point and experimental condition. These ROIs were exported by means of QuPath software (Bankhead et al., 2017). Then, ROIs were analyzed through a CellProfiler custom pipeline (Stirling et al., 2021). An indicator-based analysis and object-based methods were exploited to assess the colocalization between vaccine vectors and the intracellular vesicles. The extracted ROIs were imported into CellProfiler and split into the three related fluorescence channels. The first channel corresponding to the DAPI stain was processed through an automatic Otsu's thresholding method to generate an instance segmentation mask for each nucleus. Clustered objects were separated in single nuclei through a shape-based algorithm. The resulting multi-label nuclear mask served as a reference for single cell segmentation. A similar thresholding procedure was applied to the second channel, related to cell membranes stained with Wheat Germ Agglutinin (WGA). An Adaptive Otsu Thresholding and a propagation method were employed to accurately define the boundaries of each cell. Finally, the same threshold procedure was applied to the third channel, related to the Cy5 fluorescence signal of viral vectors, in order to obtain a binary mask. Before colocalization, fluorescence signals outside the cells were masked and removed. We exploited the "MeasureColocalization" module provided by CellProfiler, which measures colocalization and correlation between intensities on a pixel-by-pixel basis. Multiple parameters were estimated for each ROI, including Pearson's Correlation Coefficient, Overlap, and Manders' Coefficient.

Furthermore, we computed the Intersection over Union (IoU), which serves as a proxy for quantifying the overlap between the binary masks of the cells and the vaccine vector. In particular, the intersection refers to the area where the two masks overlap and contains the regions where both masks have non-zero values, identifying the pixels where both masks agree. The union represents the combined area covered by the two masks, including their overlap, and it therefore identifies the total region occupied by either of the masks. The IoU is finally computed by dividing the intersection area by the union area, returning a value between 0 (no overlap) and 1 (perfect match)

$$IoU = \frac{(VaccineVector)_{BinaryMask} \cap (Cells)_{BinaryMask}}{(VaccineVector)_{BinaryMask} \cup (Cells)_{BinaryMask}}$$

3. Results and discussion

3.1. Characterization of SLN-vaccines

The SLN-vaccines were analyzed by means of dynamic light scattering (DLS) and transmission electron microscopy (TEM) to compare the different batches and define the standard features of the formulated vaccines (Fig. 2). Moreover, further biophysical, and biochemical measurements by far UV circular dichroism (CD), RP-HPLC, and agarose gel electrophoresis were performed to characterize the formulation and the mRNA (Fig. 3). DLS was used to get information about the hydrodynamic volume of the preparation. The two vaccines exhibit a similar hydrodynamic size, and the calculated diameters are 92.89 ± 2.53 nm for Pfizer and 93.00 ± 3.00 nm for Moderna. The data were expressed in "intensity distribution" which gives information about the amount of light scattered by the particles in the different size bins (Fig. 2 A, B). In the insets, the same measurements expressed as "number distribution" give information about the number of particles in the various size bins. These results evidencing a higher polydispersity for Moderna samples. TEM pictures (Fig. 2 C-F) were also obtained from vaccines at 500 and

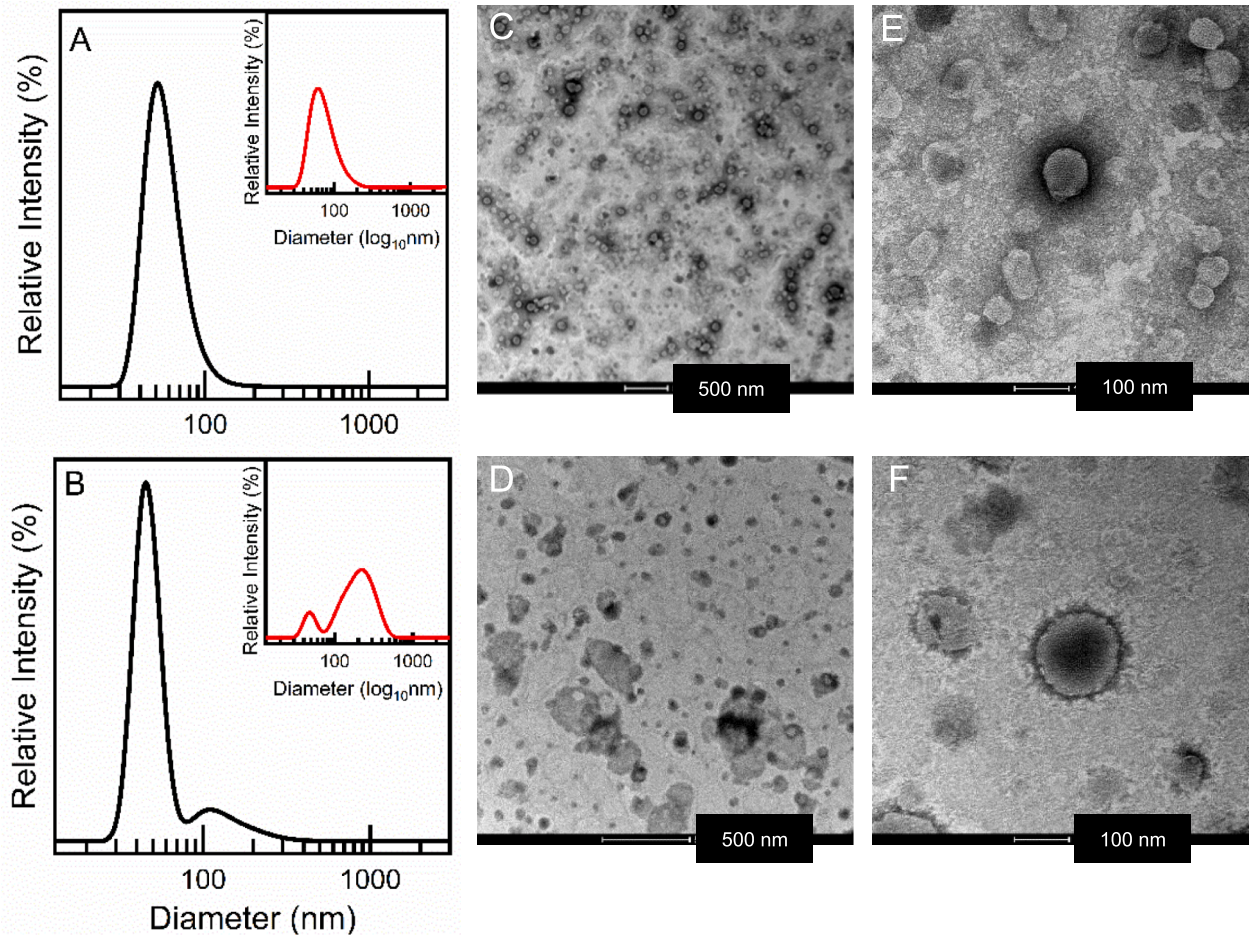

Fig. 2. Characterization of vaccines from Pfizer (upper panels) and Moderna (lower panels) by DLS (A, B) and TEM (C-F). DLS measurements were expressed as intensity distribution (black line), while in the inset the number distribution (red line) were reported. Scale bars in TEM pictures are reported on the bottom of the pictures. (For interpretation of the references to colour in this figure legend, the reader is referred to the web version of this article.)

100 nm enlargement. For Pfizer the inner diameter ranged from 14 to 160 nm, by a mean value of 49.04 ± 3.22 nm, while for Moderna the calculated median was 42.98 ± 2.18 nm.

CD spectra in the far UV region were conducted, providing information on the amount of secondary structure of RNA in SLN. Changes in the shape of the spectra were monitored as an index of RNA denaturation or structural changes. Moreover, changes of the intensity of the band at 265 nm were monitored to check differences on the oligonucleotide concentration due to its aggregation or precipitation. The shape of the CD spectra of Pfizer and Moderna vaccines recorded in their original formulation (Fig. 3, A and B, black continuous line) resembles that of standard mRNA showed in Fig. S1. Adding SDS (grey lines) or decreasing the pH (dashed lines), samples did not undergo substantial structural and concentration changes, as seen for RNA samples (Fig. S1), providing information on the protective role played by the SLN towards the environment.

Vaccine samples were loaded into a RP-HPLC column, recording the signal at 205 nm, to evaluate the lipid contribution. In Fig. 3 C, the chromatograms obtained from Pfizer (black line) and Moderna (grey line) were shown. In the plot, a main peak elutes at RT 13.6 min, and it is present in both vaccine formulations. Mass spectrometry analysis performed on the corresponding fraction reveals that it contains mainly cholesterol (Table 1). In the chromatogram relative to Pfizer samples, another peak is visible at RT 14.4 min. It was identified as azane (ALC-0159; Table 1), that is a component of the lipid nanoparticles developed for the delivery of Pfizer vaccines and was absent in Moderna vaccines (Schoenmaker et al., 2021). The runs were done recording the signal also at 260 nm and, as expected, no signals were detected at this wavelength. In Fig. 3 D is shown the agarose gel electrophoresis patterns of Pfizer and Moderna samples before (lanes 4 and 6) and after exposure to H_2O_2 to induce oxidation (lanes 5 and 7). For the two last samples, a very slight difference in migration was observed, but there is no evidence of degradation in all samples since one electrophoretic band is visible. The samples from Pfizer exhibit not resolved bands at high molecular weights, before and after the oxidation possible due to a general aggregation process. Smaller aggregates are present also in Moderna samples.

3.2. *Effect of thermal stress on the stability of SLN-vaccines*

Physical stability of SLNs vaccines Pfizer and Moderna, particularly their tendency to aggregation and degradation phenomena, was assessed through a stability study under thermal stress over a period of eight days, by measuring potential variations in the size and size distribution of the SLNs. In Fig. 4 is shown the size distribution profiles of non-diluted SLNs vaccines Pfizer (upper panel) and Moderna (lower panel) registered after (B) 4 and (C) 8 days at 40 °C and 60 % RH, in comparison to the (A) unstressed samples. No statistically significant changes in the measured parameters were registered at the conditions tested, as demonstrated by the values reported in Fig. 5D for the SLNs of both Pfizer and Moderna. Nevertheless, Moderna seems to be more resilient to physical instability phenomena than Pfizer at the conditions tested. SLNs of Moderna vaccine keep almost the same mean Z-average and PDI values over the study (respectively, 187.9 ± 0.4309 nm and

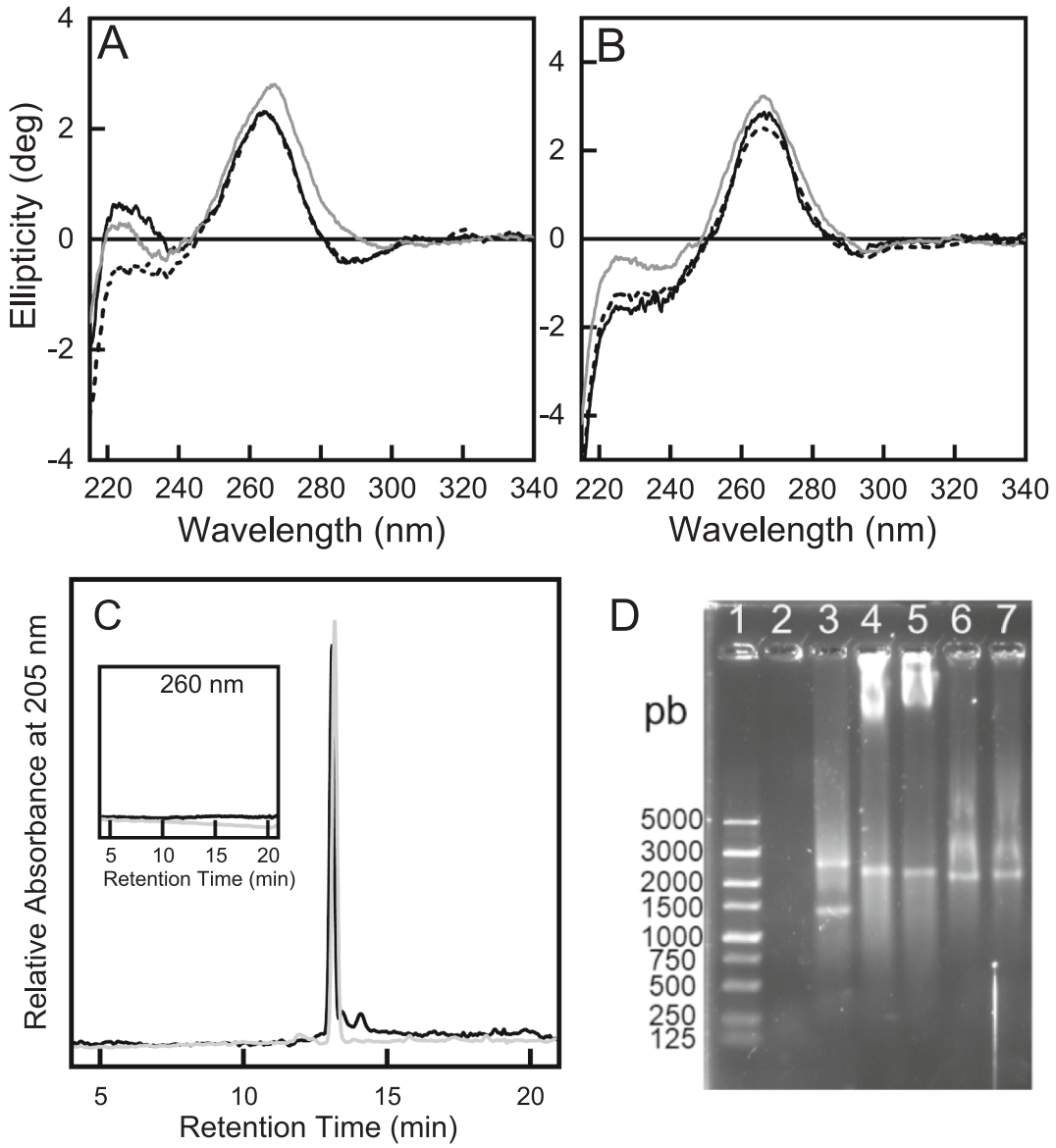

Fig. 3. Characterization of vaccines from Pfizer and Moderna by far UV CD (A, B) and by RP-HPLC (C, black and grey lines). The chromatograms were obtained recording the elution at 205 nm. The inset reports the chromatograms recorded at 260 nm. In plot D, the agarose gel was shown. CD spectra were obtained on diluted samples under different conditions: in its original formulation after dilution (black lines); in the presence of SDS (grey lines) and at pH 2.0 (dashed lines). In the gel in D samples are as follow: 1. DNA Standard 5000 bp to 125 bp, 2. Liposome, 3. RNA Broad Range standard, 4. Pfizer vaccine, 5. Pfizer after H_2O_2 treatment, 6. Moderna vaccine, 7. Moderna after H_2O_2 treatment.

Table 1
Retention time (RT) in RP-HPLC chromatogram (Fig. 3C) and molecular mass of the material corresponding to the major peaks. Mass values were determined by electrospray mass spectrometry (ESI-MS).

RP-HPLC RT (min)	*Molecular Mass (Da)*		*Chemical species*
	Found	*Calculated*	
13.6	386.61 ± 0.12	386.7	Cholesterol
14.4	542.91 ± 0.22	542.9	Azane; ALC-0159

0.181 ± 0.01546 for the unstressed sample *vs* 182.3 ± 1.735 nm and 0.174 ± 0.01275 on 8th day of the study). In the case of Pfizer vaccine, the growth of a second bigger population (~1000 nm) explains the slight increase in the Z-average parameter registered (86.35 ± 0.5841 nm and 0.2141 ± 0.0058 for the unstressed sample and 96.92 ± 0.8718 nm and 0.2495 ± 0.0055 after eight days under thermal stress). These results are also in line with the stability of these vaccines reported in other studies, in fact Moderna showed a longer stability with respect to Pfizer at room temperature (Crommelin et al., 2021; Kamiya et al., 2022).

3.3. *Effect of syringe silicon oil on the stability of SLN-vaccines*

Silicon oil is broadly used in syringes to improve the syringeability of the device. Nevertheless, its hydrophobic character could affect the physical stability of the material contained inside the syringe, inducing undesired aggregation or fusion phenomena in the specific case of SLNs. We investigated the stability of the vaccines, both Pfizer and Moderna, by measuring the size and the PDI of the SLNs after incubation in disposable sterile syringes over 90 min, to mimic the potential interaction with the silicon oil. In Fig. 5 is shown the DLS profiles obtained after (B) 10, (C) 40 and (D) 90 min of incubation inside the syringe at room temperature, both for Pfizer (upper panel) and Moderna (lower panel) vaccines. Panels (A) are representative of the unstressed samples, used as references that result in a single population with a relatively narrow

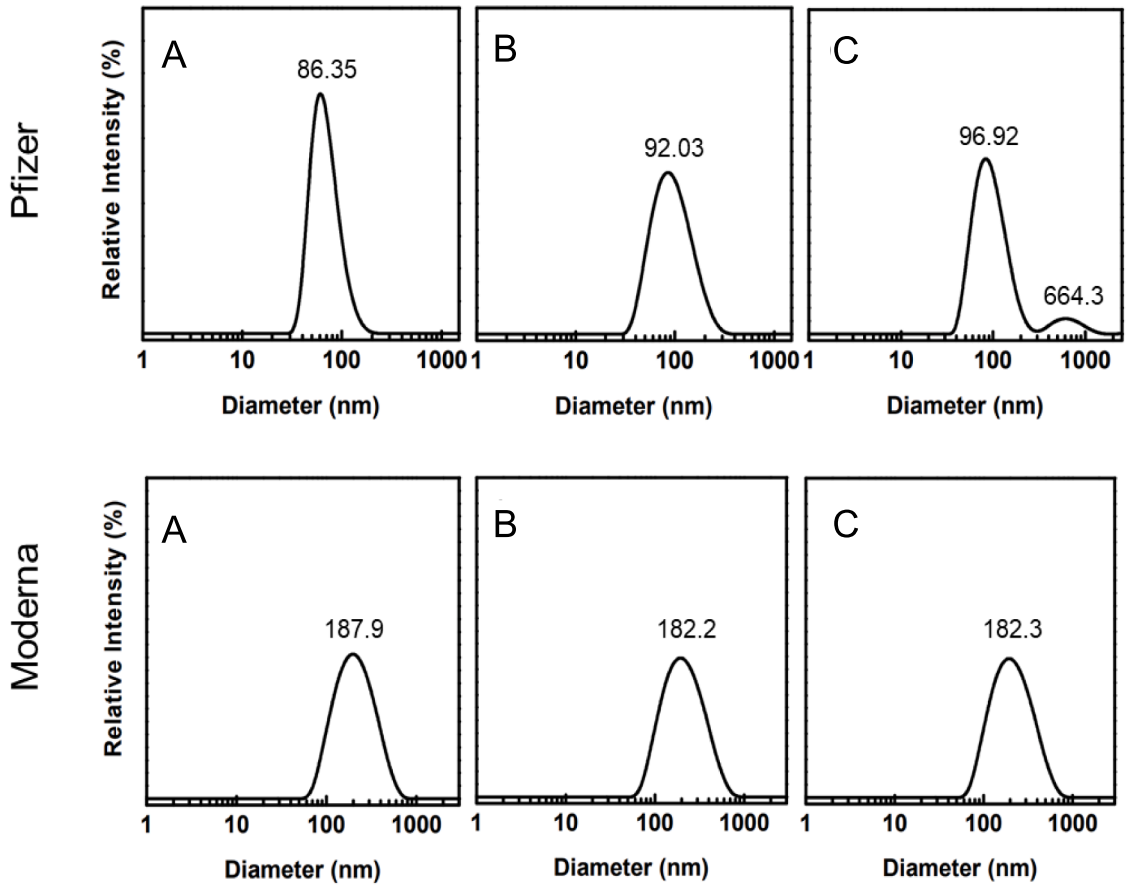

D

Vaccine	*Z-average (nm) (PDI)*		
	Unstressed sample	***4th day***	***8th day***
Pfizer	86.35 ± 0.5841 (0.2141 ± 0.0058)	92.03 ± 2,177 (0.2428 ± 0.0076)	96.92 ± 0.8718 (0.2495±0.0055)
Moderna	187.9 ± 0.4309 (0.181±0.0155)	182.2 ± 1,735 (0.1874±0.0229)	182.3 ± 1.794 (0.174 ± 0.0128)

Fig. 4. Effect of thermal stress on the size distribution by DLS of Pfizer (upper panel) and Moderna (lower panel) after (B) 4 and (C) 8 days at 40 °C, 60% room humidity (RH). Panels (A) are representative of the unstressed samples. (D) DLS measurements of vaccine samples subjected to thermal stress at 40 °C up to 8 days. Z-average (nm) and PDI values at different time points were reported. Each value is the media of three runs. Standard deviations are provided.

polydispersity (PDI $\leq$ 0.2). After 90 min of incubation inside the plastic syringe, both the samples show no statistically significant changes in the PDI (0.2141 ± 0.0058 *vs* 0.2055 ± 0.0065 and 0.181 ± 0.0155 *vs* 0.1754 ± 0.0133 for Pfizer and Moderna samples, respectively) and in the Z-average values (86.35 ± 0.5841 *vs* 87.38 ± 0.4819 and 187.9 ± 0.4309 *vs* 186.4 ± 1.951 for Pfizer and Moderna, respectively) related to the single particle distribution shown. The values are reported in Fig. 5E. The negligible variations of the measured parameters among different time points, with respect to those of the unstressed samples, corroborate that no relevant changes in size and size distributions occurred to the SLNs. These data are consistent with a strong resistance to physical instability, induced by the interaction with silicon oil, of the SLNs of both thus formulated vaccines in the conditions tested.

3.4. Effect of light on the stability of SLN-vaccines

The effect of light exposure on the stability of the SLN-vaccines in the original formulation was evaluated by using a number of biophysical and biochemical techniques. Two light doses were tested: 720 and 10460 kJ/m^2. An irradiation under 720 kJ/m^2 corresponds to about 1–2 days of solar light exposure, while the artificial solar radiation of 10460 kJ/m^2 corresponds to about 21 days of solar light exposure. This last was applied to maximize the light effect. DLS measurements demonstrate that non-irradiated (protected from light) Pfizer samples (black lines) and irradiated ones (red lines for 720 kJ/m^2 light dose and blue lines for 10460 kJ/m^2) (Fig. 6A) share quite similar hydrodynamic diameter. In the case of Moderna vaccines, the high light dose appears deleterious

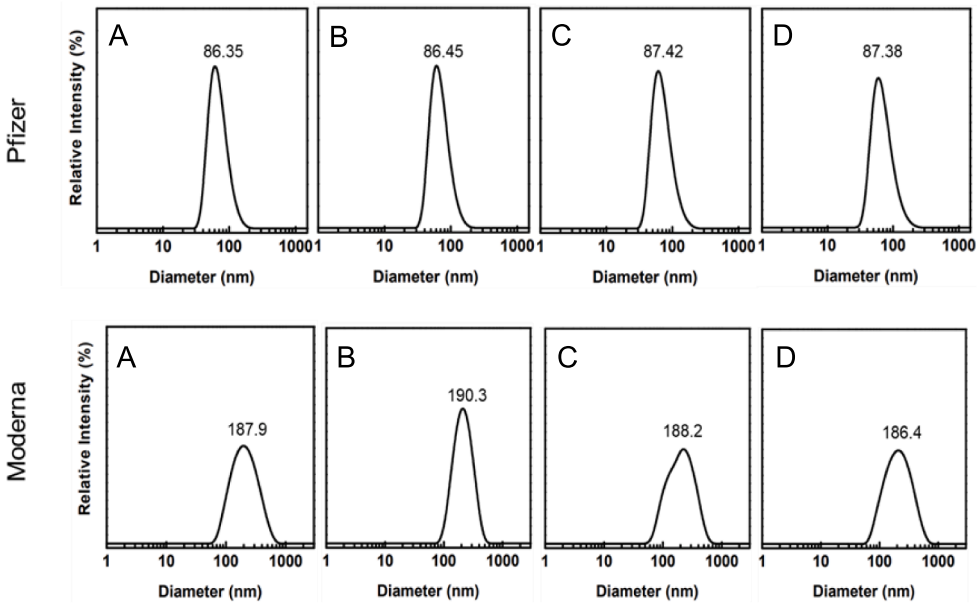

E

Vaccine	*Z-average (nm) (PDI)*			
	Unstressed sample	***10 minutes***	***40 minutes***	***90 minutes***
Pfizer	86.35 ± 0.5841 (0.2141 ± 0.0058)	86.45 ± 0.6565 (0.2107 ± 0.0313)	87.42 ± 0.2771 (0.1976 ± 0.0217)	87.38 ± 0.4819 (0.2055 ± 0.0065)
Moderna	187.9 ± 0.4309 (0.181 ± 0.0155)	190.3 ± 2.938 (0.1601 ± 0.0107)	188.2 ± 1.606 (0.15 ± 0.0270)	186.4 ± 1.951 (0.1754 ± 0.0133)

Fig. 5. Effect of interaction with silicon oil on the size distribution by DLS of Pfizer (upper panel) and Moderna (lower panel) after (B) 10, (C) 40, (D) 90 min inside disposable syringes. Panels (A) are representative of the unstressed samples. (E) DLS measurements of vaccine samples following the incubation in disposable sterile syringes over 90 min. Z-average (nm) and PDI values at different time points were reported. Each value is the media of three runs. Standard deviations are provided.

and larger aggregates of SLNs were formed (Fig. 6B). Unexpectedly, when the effects of light irradiation at the level of mRNA were investigated by agarose gel electrophoresis it appeared that the Pfizer vaccine was more sensitive. In fact, as shown in Fig. 6C, a band of mRNA at lower base pairs, about 1500 bp, is present with respect to the non-irradiated sample (Fig. 3D). The intensity of such degraded mRNA is correlated with the light dose. A similar band is also faintly visible for the Moderna vaccine only at the higher light dose. This difference can be ascribed to the different SLN sizes, bigger particle should protect better the inner mRNA with respect to the smaller SLNs, and then the SLN aggregation tendency of Moderna SLNs after light exposure (Fig. 6B) might protect the mRNA from light degradation.

The samples were also assayed by RP-HPLC. The light induces oxidation of the cholesterol contained in the lipid nanoparticles, as detected from the change in RT. When the oxidation was induced at major extent by exposing the vaccine to higher light doses (blue line), a further shift to shorter RT was observed. To confirm the oxidative phenomenon, the vaccine was treated with 5% H_2O_2 (Fig. 6E, grey lines) and similar shift in the RT of peak relative to cholesterol was observed. The mRNA structure does not appear to be affected by the light for Pfizer vaccines (Fig. 6F1), while in the CD spectrum of Moderna formulation, exposed to the higher doses of light, the intensity of the characteristic band at 265 nm is reduced, suggesting a decrease of RNA content in the sample probably related to aggregation or precipitation processes. Potentially, light-induced oxidation is quite critical for the structure of both SLN and mRNA and should be avoided, since it could lead to loss of efficacy and activity of the vaccines (Wang et al., 2019).

The mRNA quantification was conducted before and after subjecting the samples to irradiation (Fig. S2). The results showed a higher concentration of free mRNA present in equilibrium with the mRNA encapsulated within Moderna SLNs. Upon irradiation, the mRNA content in both Pfizer and Moderna SLNs appeared to decrease, with Moderna SLNs exhibiting a more pronounced reduction. This observation can be explained by considering that the mRNA located on the surface of SLNs is more susceptible to light-induced degradation due to its lack of protection. Since Moderna samples contained a higher quantity of surface mRNA, they were more susceptible to degradation caused by light exposure. The degradation of exposed mRNA due to light followed a dose-dependent pattern, emphasizing the protective role of SLNs in preserving the integrity of delivered molecules. Once outside the liposomal system, the mRNA molecules become vulnerable to degradation.

3.5. *Internalization of Pfizer and Moderna SLNs into A549 cells*

After the loading with the fluorophore and their characterization, the fluorescent SLNs were utilized to study the uptake of both COVID-19 mRNA vaccines into A549 cells stained by both Hoechst 33,258 and the WGA to visualize the cell membrane and the vesicles respectively. Although A549 are not representative cells to mimic the first target cell population following the vaccine inoculation, they have been selected because their large cytoplasm and the relevant vesicular organization enabled us to easily follow the path of fluorescent vaccines after incubation. In Fig. 7, panels A and B, representative images at three level of magnifications of cells clearly reveal that, 3 h after SLNs incubation,

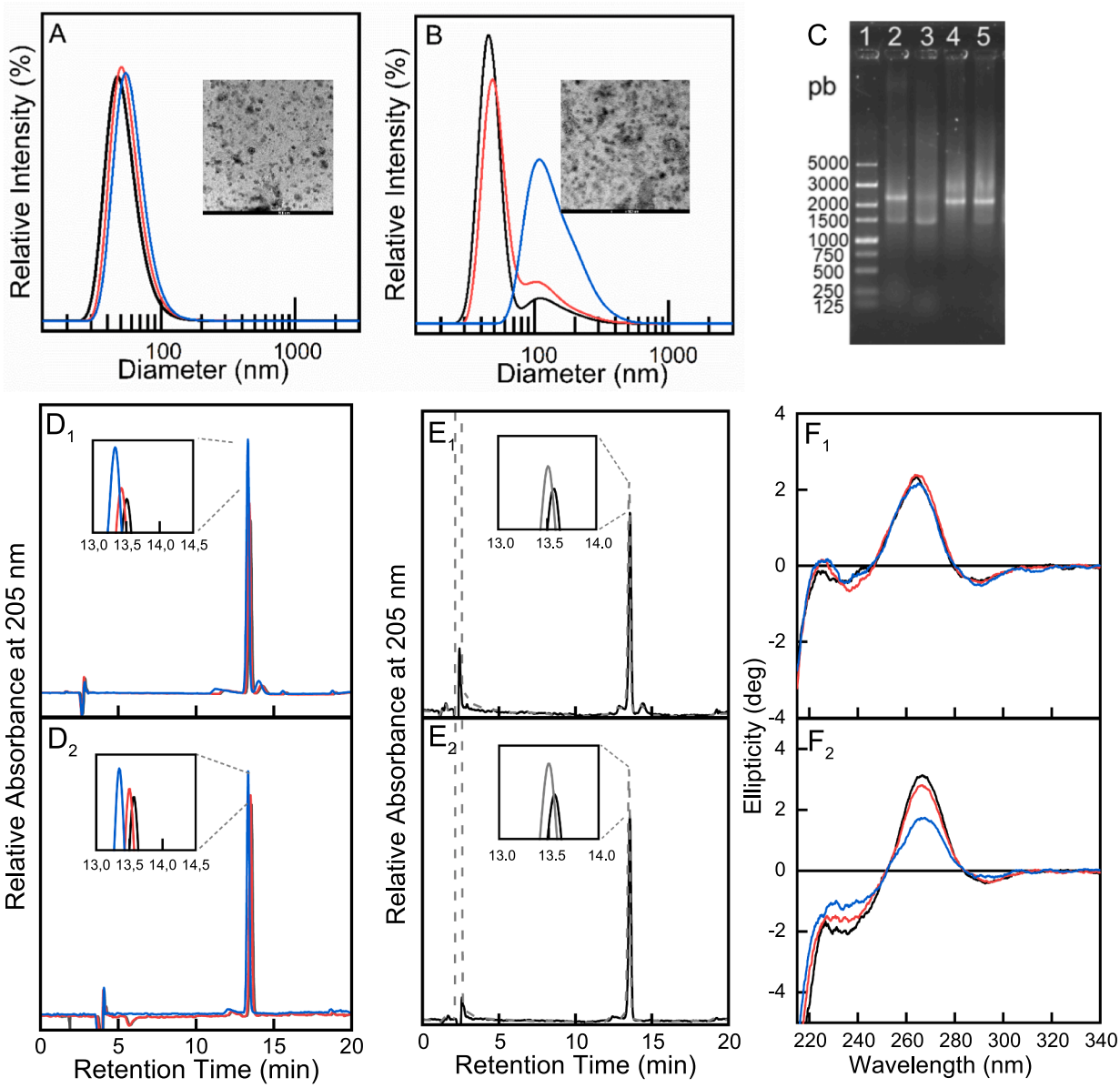

Fig. 6. Light stability of SLN vaccines probed by DLS (A, Pfizer; B, Moderna), agarose gel (C), RP-HPLC (D, E) and far UV-CD (F). Inset in A and B: TEM. Inset in D: detail of the chromatogram from 13 to 14.5 min. Black lines refer to vaccine in its formulation, red lines refer to samples irradiated with 720 kJ/m^2 artificial sun light, blue lines refer to samples irradiated with 10460 kJ/m^2 artificial sun light; grey lines refer to samples oxidized by 5% H_2O_2. Samples loaded into the gel: 1. DNA Standard 5000——125 bp, 2, 3. Pfizer samples irradiated under 720 and 10460 kJ/m^2 light, 4, 5, Moderna samples irradiated under 720 and 10460 kJ/m^2 light. (For interpretation of the references to colour in this figure legend, the reader is referred to the web version of this article.)

both Pfizer and Moderna were able to overcome the plasma membrane and penetrate inside the cell cytoplasm. In lower magnified figures (A' and B') an overview of the pattern of internalization of both SLNs (in red) in A549 cells is depicted. Interestingly, the rate of penetration in A549 differed form Pfizer and Moderna. Pfizer SLNs uptake was slower and did not involve the totality of cells at that first time-point. Conversely, almost all cells in the wells incubated with Moderna SLNs showed a red signal and the same in each cell was higher and more internalized. The images in the middle of the two panels (A'' and B'') confirmed that, independently on the kinetics of interaction with cell membrane, both formulations were able to penetrate inside the cytoplasm and to reach the perinuclear area of the cell without invading the nucleus, although Moderna had a stronger ability to invade the cytoplasm. Images at higher magnifications (A''' and B''') gave us the opportunity to distinguish among that fewer SLNs which were still interacting with the cell membranes (yellow arrows) and the others that were already internalized into the cells (red arrows). In particular, we can observe most of Pfizer SLNs into the cells and only few particles attached to the membrane, while in the case of Moderna formulation there are more particles still interacting with the cell membrane than those internalized. The higher amount of SLNs still attached to the membrane in cells treated with Moderna formulation can be considered a paradox if we consider that the uptake of Moderna SLNs was more sustained than that of Pfizer formulation. However, it can be due to a limited availability of endosomal vesicles that, somehow, delay the continuous flux of nanoparticles from the membrane to the cell cytoplasm. The ability of SLNs associated with mRNA to be internalized in cells has been widely reported (Liang et al., 2017), and the success of the vaccine campaign indirectly confirmed the ability of both formulations to be internalized in cells after the intramuscular injection. In addition, the present study allowed us to visualize the pattern of intercellular distribution of these two vaccines and, to determine their interaction

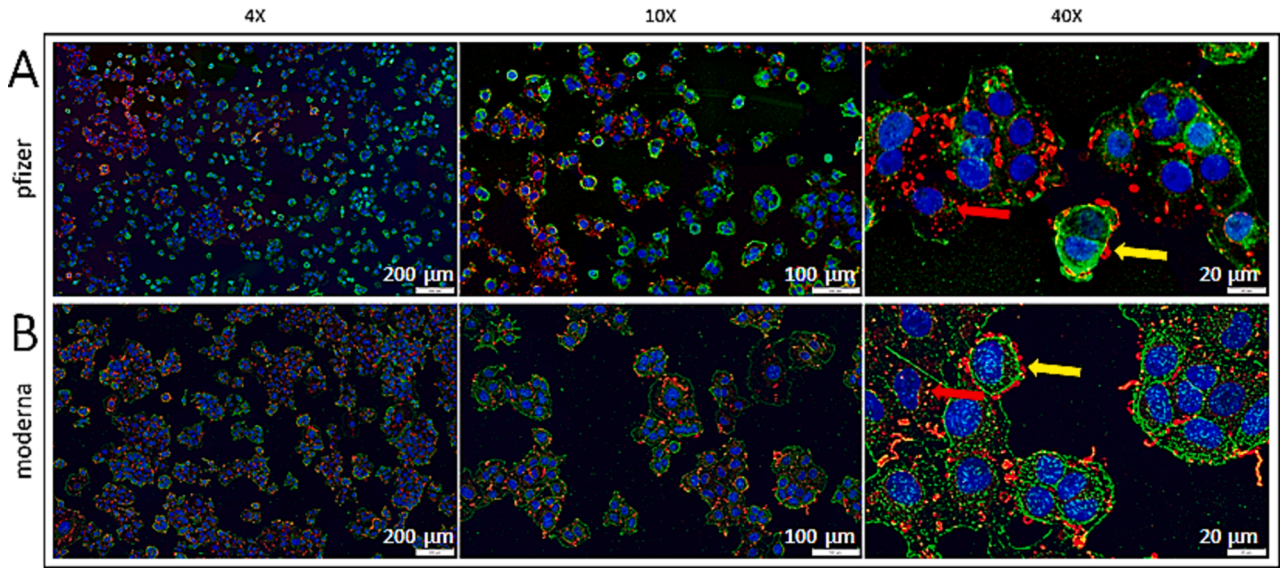

Fig. 7. Representative images of A549 cells treated for 3 h with Pfizer (upper images, panel A) or Moderna (lower images, panel B) SLNs. Plasma membranes and intracellular vesicles were stained with WGA488 (green signal) and nuclei with Hoechst 33,258 (blue signal). The red signal was associated with the presence of DiD (red signal). Images were acquired with Virtual Slide Olympus VS120 microscope at three different magnifications. Scale bar: Left column = 200 µm; middle column = 100 µm; right column = 20 µm. (For interpretation of the references to colour in this figure legend, the reader is referred to the web version of this article.)

with cytoplasmic vesicles.

Since the mechanism of entry of SLNs is an endocytic pathway guided by retrograde transport of endosomal vesicles, and the mRNA transcription of spike protein is tightly correlated to the process of endosomal escape of SLNs, we performed a detailed measurement of the colocalization of SLNs with intracellular vesicles at three different time-points, 3-, 24- and 96-hours. In Fig. 8A, a representative high magnified image of a single A549 cell incubated for 24 h with Pfizer's vaccine, is shown. For each image, saved at the same magnification, 6 different squares having the same area, were randomly selected as reported in Fig. 8B. This step was crucial to calculate the rate of colocalization by the Pearson correlation coefficient "r" (see f Fig. 8C). The analysis of the quantification revealed that similarly to what is reported in Fig. 7, the fast and strong process of internalization of Moderna SLNs was followed by a rather rapid escape from the endosomes, as demonstrated by a very low percentage of colocalization (around the 10%) at three hours after incubation. Our study also showed that, at the same time-point, the percentage of colocalization for Pfizer SLNs was higher than that from Moderna SLNs. This could suggest either a slower release from endosomes or a faster accumulation in lysosomes for Pfizer SLNs with respect to Moderna SLNs. The drastic decrease of colocalization at the following time-points mostly indicates that Pfizer SLNs remain for a longer time in retrieval vesicles, but they can be efficiently released even 24 h after cell penetration. Quite interestingly, the cells treated with Moderna SLNs showed an opposite behaviour in which the colocalization is increased at 24 h and 96 h timepoints with respect to that at 3 h.

Vaccination using SLNs is hypothesized to induce an efficient endosomal escape before being degraded by lysosomal enzymes. The proton sponge effect is the most commonly used strategy to enhance endosomal escape. The ability of polymer-based NPs such as polyethyleneimine (PEI) and PAMAM dendrimers has already been shown to be highly efficient for this process (Pearson et al., 2014). After endosomal escape, both vaccines can reach the perinuclear area, as clearly shown in Fig. 7A-B, 8A or they can enter either in lysosomal vesicles. The maturation of lysosomes often leads to their fusion and externalization exocytotic bodies. Although immunofluorescence staining directed

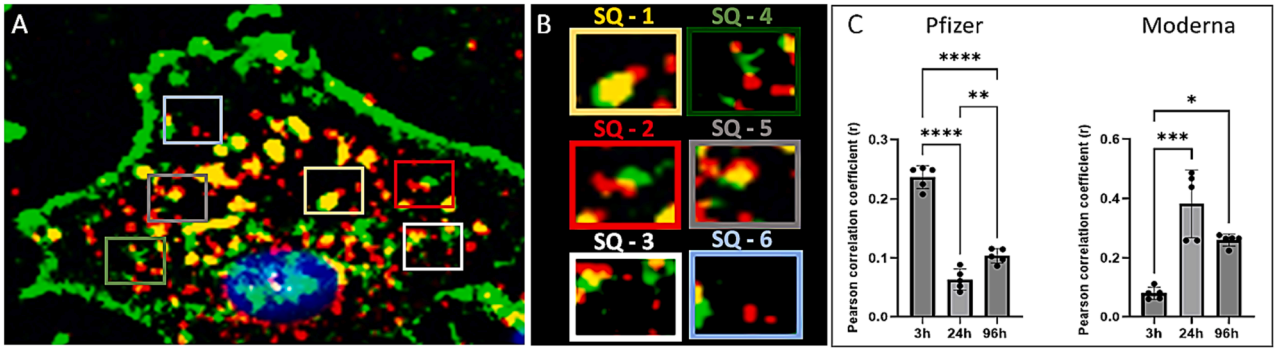

Fig. 8. Panel A: representative image of a single A549 cell (blue signal, nucleus, green signal plasma membrane and intracellular vesicles) incubated for 24 h with Pfizer SLNs (red signal). Panel B: higher magnification of the 6 selected squares depicted in the panel A (three colours can be seen, green, red, and yellow as overlapping of the two previous signals). For each image, acquired through Virtual Slide Olympus VS120 microscope, 6 different squares having the same area and randomly selected as reported in figure to calculate the rate of colocalization. For each square the percentage of colocalization was calculated as follows: $\frac{numberofyellowpixels}{(numberofredpixels+numberofyellowpixels)} x100$. Panel C histogram showing the Pearson correlation coefficient at the three different time-points (3 h, 24 h and 96 h). The studies were carried out through Cell Profiler Software. Data are reported as mean ± S.D and the value of each single measurement was reported as plot. Statistical analysis performed with 2Way Anova test (Tukey post hoc). ****p value < 0.0001 ***p value < 0.001 **p value < 0.01 *p value < 0.1, using Prism 5 (GraphPad 9.2). (For interpretation of the references to colour in this figure legend, the reader is referred to the web version of this article.)

against the different vesicles (e.g., early endosomes or mature lysosomes) was not performed, it is quite presumably that the higher colocalization level found at 24- and 96- hours after Moderna SLNs incubation was due to a secondary entrapment of SLNs by exocytotic system (e.g., lysosomes, autophagosomes, multi vesicular bodies). This hypothesis is furthermore strengthen by our recent studies carried out with TEM showing that gold nanoparticles tha were observed either freely circulating in the cytoplasm or entrapped in in exocytotic bodies, such (Gustà et al., 2023). Interestingly this mechanism was also observed in cells exposed to polystyrene nanoparticles (Liu et al., 2023) or softer materials (Zhang et al., 2020). It is therefore extremely likely that endosome/multivesicular late endosomes may serve as a transient reservoir where NPs recycle through multiple pathways. This process can explain how both Moderna and Pfizer SLNs may interact with cells at subcellular level.

Independently on the final fate of SLNs, the present study also suggested that fluorescent vaccines can be easily detected inside the cells and that they are able to be rapidly internalized, escape from the endosomes and remain inside the cytoplasm.

4. Conclusion

The mRNA-SLN vaccine platform has emerged as a promising approach to transporting and delivering mRNA to cells, with a number of clinically investigated mRNA-SLN formulations showing improved selectivity and reduced toxicity, mainly for cancer treatment (Schwendener, 2014). The potential of using nucleic acid-based therapies for treating human diseases has been enticing for a long time, but the progresses were limited owing to issues like easily degradation by nucleases in vivo and difficulties in reaching the target cells. The latest successful application of SLN was in the delivery of spike mRNA in COVID-19 vaccines, which has been fundamental in preventing the disease and combating the SARS-CoV2 pandemic. In fact, mRNA vaccines have revolutionized the concept of vaccines and their development, showing incredible high efficacy and potential low-cost production thanks to SLN-based technologies to deliver nucleic acids.

However, the need to simplify the use of vaccines and promote large-scale vaccination globally has raised the problem of the stability of these mRNA-SLNs. Processing biopharmaceuticals in the GMP setting exposes these molecules to a series of possible stresses, including freeze-thawing, dilution, agitation, and others. In particular, limited data are available about the photosensitivity of this class of therapeutics. While various groups have described the UV light mediated degradation of protein drugs, especially under UV conditions selected by the ICH Q1B recommendations, there is limited information on mRNA vaccines.

In this article, we have considered the stability of Pfizer and Moderna vaccines to three stressors. While thermal stress and syringe-derived oil exposition seem to have little effect on the stability of the SLN vaccines, light appears potentially dangerous. Our study has demonstrated the protective effects of the SLN system on mRNA vaccines against damage mediated by light exposure, supporting the idea that SLN could potentially be used as a scavenger to prevent light-induced damage. Moreover, the in vitro internalization study showed that some well detectable differences among Moderna and Pfizer SLNs can be revealed in terms of internalization rate and endosomal escape, in spite of their similar physical–chemical features.

Declaration of Competing Interest

The authors declare that they have no known competing financial interests or personal relationships that could have appeared to influence the work reported in this paper.

Data availability

Data will be made available on request.

Acknowledgements

GP and BC were supported by "Fondazione Cariparo" [Grant number 55828; 2020]. This study was conducted in the ambit of a project between University of Padova and “ULSS 3 Serenissima”, Mestre Hospital.

Appendix A. Supplementary material

Supplementary data to this article can be found online at https://doi.org/10.1016/j.ijpharm.2023.123319.

References

Alameh, M.G., Weissman, D., Pardi, N., 2022. Messenger RNA-based vaccines against infectious diseases. Curr. Top. Microbiol. Immunol. 440, 111–145. https://doi.org/10.1007/82_2020_202.

Arteta, M.Y., Kjellman, T., Bartesaghi, S., Wallin, S., Wu, X., Kvist, A.J., Dabkowska, A., Székely, N., Radulescu, A., Bergenholtz, J., Lindfors, L., 2018. Successful reprogramming of cellular protein production through mRNA delivered by functionalized lipid nanoparticles. PNAS 115, E3351–E3360. https://doi.org/10.1073/PNAS.1720542115.

Bankhead, P., Loughrey, M.B., Fernández, J.A., Dombrowski, Y., McArt, D.G., Dunne, P. D., McQuaid, S., Gray, R.T., Murray, L.J., Coleman, H.G., James, J.A., Salto-Tellez, M., Hamilton, P.W., 2017. QuPath: Open source software for digital pathology image analysis. Sci. Reports 7 (1), 1–7. https://doi.org/10.1038/s41598-017-17204-5.

Crommelin, D.J.A., Anchordoquy, T.J., Volkin, D.B., Jiskoot, W., Mastrobattista, E., 2021. Addressing the Cold Reality of mRNA Vaccine Stability. J. Pharm. Sci. 110, 997–1001. https://doi.org/10.1016/J.XPHS.2020.12.006.

Duan, L., Zheng, Q., Zhang, H., Niu, Y., Lou, Y., Wang, H., 2020. The SARS-CoV-2 Spike Glycoprotein Biosynthesis, Structure, Function, and Antigenicity: Implications for the Design of Spike-Based Vaccine Immunogens. Front. Immunol. 11 https://doi.org/10.3389/FIMMU.2020.576622.

Geall, A.J., Verma, A., Otten, G.R., Shaw, C.A., Hekele, A., Banerjee, K., Cu, Y., Beard, C. W., Brito, L.A., Krucker, T., O'Hagan, D.T., Singh, M., Mason, P.W., Valiante, N.M., Dormitzer, P.R., Barnett, S.W., Rappuoli, R., Ulmer, J.B., Mandl, C.W., 2012. Nonviral delivery of self-amplifying RNA vaccines. PNAS 109, 14604–14609. https://doi.org/10.1073/PNAS.1209367109/-/DCSUPPLEMENTAL/PNAS.201209367SI.PDF.

Granados-Riveron, J.T., Aquino-Jarquin, G., 2021. Engineering of the current nucleoside-modified mRNA-LNP vaccines against SARS-CoV-2. Biomed. Pharmacother. 142 https://doi.org/10.1016/J.BIOPHA.2021.111953.

Gustà, M.F., Edel, M.J., Salazar, V.A., Alvarez-Palomo, B., Juan, M., Broggini, M., Damia, G., Bigini, P., Corbelli, A., Fiordaliso, F., Barbul, A., Korenstein, R., Bastús, N. G., Puntes, V., 2023. Exploiting endocytosis for transfection of mRNA for cytoplasmatic delivery using cationic gold nanoparticles. Front. Immunol. 14 https://doi.org/10.3389/FIMMU.2023.1128582.

Hald Albertsen, C., Kulkarni, J.A., Witzigmann, D., Lind, M., Petersson, K., Simonsen, J. B., 2022. The role of lipid components in lipid nanoparticles for vaccines and gene therapy. Adv. Drug Deliv. Rev. 188 https://doi.org/10.1016/J.ADDR.2022.114416.

Kamiya, M., Matsumoto, M., Yamashita, K., Izumi, T., Kawaguchi, M., Mizukami, S., Tsurumaru, M., Mukai, H., Kawakami, S., 2022. Stability Study of mRNA-Lipid Nanoparticles Exposed to Various Conditions Based on the Evaluation between Physicochemical Properties and Their Relation with Protein Expression Ability. Pharmaceutics 14. https://doi.org/10.3390/PHARMACEUTICS14112357.

Kowalski, P.S., Rudra, A., Miao, L., Anderson, D.G., 2019. Delivering the Messenger: Advances in Technologies for Therapeutic mRNA Delivery. Mol. Ther. 27, 710–728. https://doi.org/10.1016/J.YMTHE.2019.02.012.

Kulkarni, J.A., Cullis, P.R., Van Der Meel, R., 2018. Lipid Nanoparticles Enabling Gene Therapies: From Concepts to Clinical Utility. Nucleic Acid Ther. 28, 146–157. https://doi.org/10.1089/NAT.2018.0721.

Liang, F., Lindgren, G., Lin, A., Thompson, E.A., Ols, S., Röhss, J., John, S., Hassett, K., Yuzhakov, O., Bahl, K., Brito, L.A., Salter, H., Ciaramella, G., Loré, K., 2017. Efficient Targeting and Activation of Antigen-Presenting Cells In Vivo after Modified mRNA Vaccine Administration in Rhesus Macaques. Mol. Ther. 25, 2635. https://doi.org/10.1016/J.YMTHE.2017.08.006.

Linkert, M., Rueden, C.T., Allan, C., Burel, J.M., Moore, W., Patterson, A., Loranger, B., Moore, J., Neves, C., MacDonald, D., Tarkowska, A., Sticco, C., Hill, E., Rossner, M., Eliceiri, K.W., Swedlow, J.R., 2010. Metadata matters: access to image data in the real world. J. Cell Biol. 189, 777–782. https://doi.org/10.1083/JCB.201004104.

Liu, Y.Y., Liu, J., Wu, H., Zhang, Q., Tang, X.R., Li, D., Li, C.S., Liu, Y., Cao, A., Wang, H., 2023. Endocytosis, Distribution, and Exocytosis of Polystyrene Nanoparticles in Human Lung Cells. Nanomaterials 13, 84. https://doi.org/10.3390/NANO13010084/S1.

Pardi, N., Hogan, M.J., Porter, F.W., Weissman, D., 2018. mRNA vaccines — a new era in vaccinology. Nat. Rev. Drug Discov. 17, 261–279. https://doi.org/10.1038/nrd.2017.243.

Pearson, R.M., Hsu, H.J., Bugno, J., Hong, S., 2014. Understanding nano-bio interactions to improve nanocarriers for drug delivery. MRS Bull. 39, 227–237. https://doi.org/10.1557/MRS.2014.9.

Polack, F.P., Thomas, S.J., Kitchin, N., Absalon, J., Gurtman, A., Lockhart, S., Perez, J.L., Pérez Marc, G., Moreira, E.D., Zerbini, C., Bailey, R., Swanson, K.A.,

Roychoudhury, S., Koury, K., Li, P., Kalina, W.V., Cooper, D., Frenck, R.W., Hammitt, L.L., Türeci, Ö., Nell, H., Schaefer, A., Ünal, S., Tresnan, D.B., Mather, S., Dormitzer, P.R., Şahin, U., Jansen, K.U., Gruber, W.C., 2020. Safety and Efficacy of the BNT162b2 mRNA Covid-19 Vaccine. N. Engl. J. Med. 383, 2603–2615. https://doi.org/10.1056/NEJMOA2034577.

Ramachandran, S., Satapathy, S.R., Dutta, T., 2022. Delivery Strategies for mRNA Vaccines. Pharmaceut. Med. 36, 11–20. https://doi.org/10.1007/S40290-021-00417-5.

Schoenmaker, L., Witzigmann, D., Kulkarni, J.A., Verbeke, R., Kersten, G., Jiskoot, W., Crommelin, D.J.A., 2021. mRNA-lipid nanoparticle COVID-19 vaccines: Structure and stability. Int. J. Pharm. 601 https://doi.org/10.1016/J.IJPHARM.2021.120586.

Schwendener, R.A., 2014. Liposomes as vaccine delivery systems: a review of the recent advances. Ther. Adv. Vaccines 2, 159. https://doi.org/10.1177/2051013614541440.

Stirling, D.R., Swain-Bowden, M.J., Lucas, A.M., Carpenter, A.E., Cimini, B.A., Goodman, A., 2021. Cell Profiler 4: improvements in speed, utility and usability. BMC Bioinf. 22, 1–11. https://doi.org/10.1186/S12859-021-04344-9/FIGURES/6.

Tenchov, R., Bird, R., Curtze, A.E., Zhou, Q., 2021. Lipid Nanoparticles from Liposomes to mRNA Vaccine Delivery, a Landscape of Research Diversity and Advancement. ACS Nano 15, 16982–17015. https://doi.org/10.1021/ACSNANO.1C04996/ASSET/IMAGES/MEDIUM/NN1C04996_0026.GIF.

Wang, C., Siriwardane, D.A., Jiang, W., Mudalige, T., 2019. Quantitative analysis of cholesterol oxidation products and desmosterol in parenteral liposomal pharmaceutical formulations. Int. J. Pharm. 569 https://doi.org/10.1016/J.IJPHARM.2019.118576.

Zhang, M., Liu, L., Lin, X., Wang, Y., Li, Y., Guo, Q., Li, S., Sun, Y., Tao, X., Zhang, D., Lv, X., Zheng, L., Ge, L., 2020. A Translocation Pathway for Vesicle-Mediated Unconventional Protein Secretion. Cell 181, 637–652.e15. https://doi.org/10.1016/J.CELL.2020.03.031.

Zhu, N., Zhang, D., Wang, W., Li, X., Yang, B., Song, J., Zhao, X., Huang, B., Shi, W., Lu, R., Niu, P., Zhan, F., Ma, X., Wang, D., Xu, W., Wu, G., Gao, G.F., Tan, W., 2020. A Novel Coronavirus from Patients with Pneumonia in China, 2019. N. Engl. J. Med. 382, 727–733. https://doi.org/10.1056/NEJMOA2001017.